# Dynamics of surface currents over Qingdao coastal waters in August 2008

Jian Zhao,[1,2] Xueen Chen,[1] Wei Hu,[3] Jinrui Chen,[1] and Mingke Guo[3]

Received 10 January 2011; revised 22 July 2011; accepted 27 July 2011; published 15 October 2011.

[1] Surface currents measured by High Frequency (HF) radar are used to investigate the dynamics in the coastal waters of Qingdao, China, on the western coast of the Yellow Sea. Different factors affecting the surface currents are revealed by dynamical analysis. Harmonic tidal analysis shows that the coastal tidal currents are barotropic and their temporal evolution is mainly influenced by the semidiurnal tidal constitutes, topography and geometry. It is also found that their horizontal distribution represents the effect of local topography. At sub-tidal frequencies, the high correlation between winds and the sub-tidal surface currents indicates a crucial role of wind-forcing in driving the currents. Varying wind direction coupled with small-scale features of the coastal geometry results in complicated sub-mesoscale circulation. In addition, the monthly coastal circulation is characterized by an eddy structure and is primarily determined by the outflow which is closely associated with the sea level slope along the coast. The variability of the residual currents is studied by analyzing the cross-shore momentum equation with wind stress, sea level records, and HF radar currents. It is shown that both the barotropic pressure gradient and the nonlinear tidal stress contribute to the variations of the residual currents near the bay mouth and further govern the coastal monthly circulation in August, 2008.

**Citation:** Zhao, J., X. Chen, W. Hu, J. Chen, and M. Guo (2011), Dynamics of surface currents over Qingdao coastal waters in August 2008, *J. Geophys. Res.*, *116*, C10020, doi:10.1029/2011JC006954.

## 1. Introduction

[2] Qingdao coastal waters and Jiaozhou Bay are located on the western coast of the Yellow Sea (YS), P. R. China. Jiaozhou Bay is a shallow, semi-closed bay with a total area of about 350 km$^2$ and has an average water depth of 7 m [*Chen et al.*, 1999; *Liu et al.*, 2007]. There is a deep channel in the mouth of Jiaozhou Bay, which plays a critical role in the water discharge between Jiaozhou Bay and Qingdao coastal waters (Figure 1).

[3] Since the 1980s, many cruises were conducted in this coastal area to study the distribution and the variability of coastal currents, temperature, salinity, primary productivity as well as nutrients [*Pan et al.*, 1995; *Zhang and Sheng*, 1997; *Yang and Wu*, 1999; *Sun et al.*, 2005]. Some previous observations in this region were summarized in *Physical Environments of Jiaozhou Bay* [*First Institute of Oceanography of SOA*, 1984] and *Annals of Bays in China* [*Editorial Board of Annals of Bays in China*, 1993]. It was observed that the currents in Qingdao coastal waters were dominated by semidiurnal tidal currents. Due to the shallow water depth and complex geometry, the tidal currents were featured by mostly barotropic structure and spatial dependence. Near the entrance of Jiaozhou Bay, residual currents reached about 10–50 cm s$^{-1}$ [*Lu et al.*, 2008], and the maximum tidal speed exceeded 100 cm s$^{-1}$ [*Lozovatsky et al.*, 2008a].

[4] However, historical observations are scattered in temporal and spatial distribution. The fragmentary nature of the measurements makes it difficult to fully understand the coastal dynamics in this area, including the spatial structure of the tidal currents and the variability of sub-tidal currents. Despite a series of numerical studies focused on the tidal currents and the influences of local physical processes on the ecosystem [*Wang et al.*, 1980; *Bao et al.*, 1999; *Chen et al.*, 1999; *Yan et al.*, 2001; *Liu et al.*, 2004; *Lü and Qiao*, 2008], the dynamically temporal and spatial structure of the Qingdao coastal currents have not been well understood. For example, the time scale for wind-driven currents and the response of sea surface currents to local wind-forcing are still unclear. Lack of long-term observations also impede the understanding about the variability on longer time scales. In 2008, a high frequency (HF) radar arrays monitoring system was installed around the coastal areas of Qingdao. It measured ocean surface currents over a large area with short intervals, providing an unprecedented view of the surface currents off the coastal ocean, particularly about the sub-mesoscale circulation. In addition, the

[1]College of Physical and Environmental Oceanography, Ocean University of China, Qingdao, China.
[2]Division of Meteorology and Physical Oceanography, Rosenstiel School of Marine and Atmospheric Science, University of Miami, Miami, Florida, USA.
[3]North China Sea Marine Forecasting Center, State Oceanic Administration, Qingdao, China.


0148-0227/11/2011JC006954

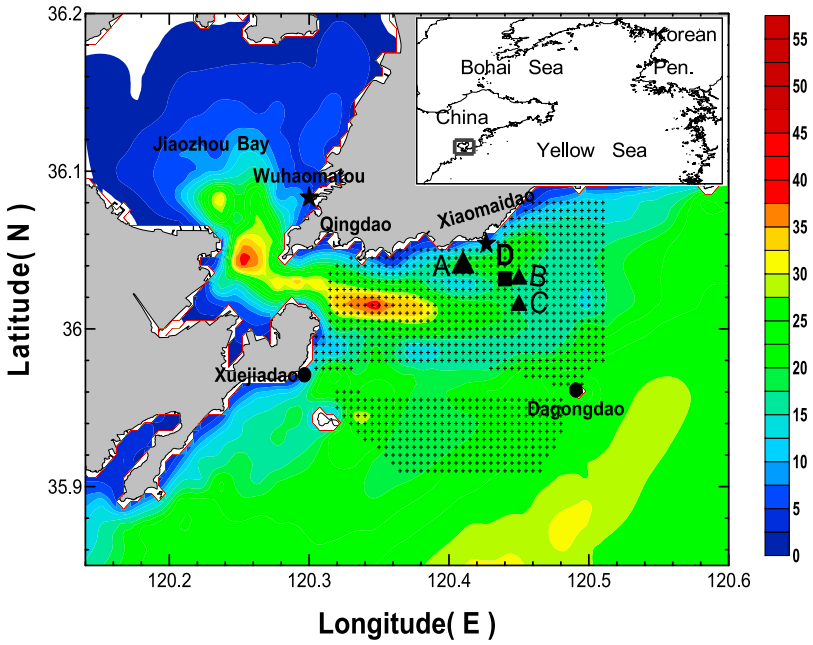


**Figure 1.** General area of study and data locations. Bathymetry contours (solid lines) are in meters. Instrument locations are indicated as follows: HF radar (CODAR) instruments (dots); radar grids (criss-cross); buoys (solid triangles); tide gauge stations (solid pentacle); ADP (solid square). Qingdao represents Qingdao Baguanshan meteorological station.

sufficient long time series from the HF radar units enable us to explore the variability over different frequency.

[5] Dynamical factors primarily controlling the temporal and spatial variations of the coastal currents near Jiaozhou Bay include tides, wind and river discharge. It is proposed that the semidiurnal M2 tidal motions contribute about 80% of the kinetic and potential energy inside the bay [*Ding*, 1992]. Wind-driven current is also an essential component of the surface currents. Surface winds near Jiaozhou Bay are modulated by the Asian Monsoon, and the changes of wind speed and direction would definitely affect the near surface currents and even the coastal circulation pattern. Furthermore, there are six major rivers around Jiaozhou Bay with a maximum discharge of 135 $m^3$ $s^{-1}$ occurring in August [*Marine Environmental Monitoring Center*, 1992]. Monsoon and the costal estuarine outflows lead to sea level rising by about 50 cm through a seasonal cycle [*Pu et al.*, 2004]. However, the sea level has irregular distribution along the coast, resulting from the special geometry around Jiaozhou Bay. During summer, the sea surface height of the inner bay is generally higher than the outside with sea level differences about 5 cm in June, 4 cm in July and 1 cm in August. As *Pu et al.* [2004] stated, the pressure gradient generated by the sea surface slope across Jiaozhou Bay has important dynamical impact on the alongshore currents.

[6] Those factors mentioned above result in sophisticated variations in the coastal circulation. Analysis of the momentum equation is necessary to identify the dominant processes for the coastal dynamics. The momentum balance on monthly scale reveals the crucial role of the coastal sea surface slope in governing the nearshore monthly circulation [*Pu et al.*, 2004]. On daily timescale, however, there should be different mechanisms, since a lot of studies have proven that the nonlinear tidal stress greatly contribute to the residual circulation [*Visser et al.*, 1990; *Jay and Smith*, 1990; *Winant*, 2008]. It is noteworthy that the transition of tidal stress over spring-neap cycles might give rise to the variability of Eulerian residual circulation [*Stacey et al.*, 2010]. A similar momentum analysis will also be performed in this paper to examine the key processes responsible for the coastal variability.

[7] In this study, the coastal surface circulation off Qingdao is dynamically investigated based on the new measurements from two high-frequency radar units during August 2008. The interaction between tides, topography and geometry will be pointed out, and the response of sea surface currents to local wind is also studied. Additional analysis about the momentum balance in cross-shore direction will be performed to quantify the effects of tides, wind and the estuarine discharge on modulating the daily variations of the water exchanges between Jiaozhou Bay and the coastal waters.

[8] This article is organized as follows. A brief description of observational data sets is given in the following section. In section 3, the validation of measurements used in this paper is described, followed by analysis of the tidal currents, wind driven currents, and monthly coastal circulation in section 4. Factors controlling the momentum balance near the entrance of Jiaozhou Bay are evaluated in section 5. Finally, this paper is concluded with a summary and some further discussions.

## 2. Data

### 2.1. HF Radar Data

[9] The surface currents used in this paper are measured by a HF radar monitoring system. These HF radars are SeaSonde units produced by CODAR Ocean Sensors, and

consist of three parts, including two radar stations and a data processing center. Each radar station is composed of a transmitting antenna and a receiving antenna. Two radar stations are located at Xuejiadao and Dagongdao (Figure 1), respectively, spaced 22 km apart. They operate at a central frequency near 25 MHz and imply averaged near surface currents over the upper 0.5–1 m of the water column.

[10] When hitting sea surface, the electromagnetic waves from the transmitting antenna will be backscattered off the ocean surface by Bragg scattering mechanism. Reflected signal will then be collected by the receiving antenna. The Doppler shift, refer to the difference between the transmitted and received frequency, is used to calculate the radial currents with respect to each radar station. Further details regarding data processing method can be found in previous literature [*Barrick et al.*, 1977; *Lipa and Barrick*, 1983; *Paduan and Rosenfeld*, 1996; *Paduan and Graber*, 1997; *Paduan and Cook*, 1997].

[11] In the data processing center, radial current maps from two radar units were combined to estimate the velocity vectors, which were converted into hourly maps on 0.5 km by 0.5 km regular grid. Radial data within a 1 km radius of the grid point were used to derive vector maps. Corrections for measured deviations from ideal radar pattern were performed at each radial site. The coverage area of the HF radar extended approximately 400 $km^2$. The HF radar monitoring system was successfully operated for the period from July 20 to September 3 in 2008. The continuous and high-quality surface currents, with the maximum gap less than 5 h, were obtained from July 30 to September 1 (33 days).

[12] To derive reliable sea surface current vectors, the raw time series were preprocessed grid by grid. The vectors with amplitudes greater than 2.0 m $s^{-1}$ or with geometric dilution of precision (GDOP) greater than 1.5 were rejected. The variability of measured currents was also carefully examined. At each grid point, if its magnitude on one time step deviated from its temporal mean larger than twice of the standard deviations, this time step was discarded. Finally, only grid points whose valid data were available more than 80% of the temporal coverage were included in this study. The spatial distribution of the temporal percent coverage is shown in Figure 2. Over the northern part of the area under study, most grid points had more than 90% available data. Similarly, valid data in the southern part also exceeded 80% (Figure 2). Data coverage in the region that directly connects the radar stations was poor since they lie on the co-linearity of two radar stations [*Schmidt*, 1986; *Barrick and Lipa*, 1996; *de Paolo and Terrill*, 2007]. Those data were also eliminated and resulted in undesirable spatial discontinuities of the surface currents field. Linear interpolation was applied for gaps with length of a few hours to obtain sequential currents.

### 2.2. ADP Currents

[13] A bottom-mounted SonTek/YSI ADP (Acoustic Doppler Profiler) was deployed off the Qingdao coast from 16 March to 17 April, 2008 to measure the vertical distribution of the coastal currents (Figure 1). The upward-looking ADP measured currents with 250 kHz and sampling temporal interval 5 min, vertical resolution 1.7 m. Mooring ADP was located at 36°1′54.7″N and 120°27′14″E, inside the region covered by HF radar. Although the observational time of the ADP and HF radar did not overlap, tidal currents accounted for about 80% of the kinetic variations in this region and some tidal characteristics did not change dramatically with time. Measurements from ADP will serve as an independent comparison for HF radar currents, and also be used to investigate the vertical distribution of the tidal ellipses.

### 2.3. Buoy Data

[14] Hourly observations were available from three buoys (A, B, and C) maintained by *North China Sea Marine Forecasting Center of State Oceanic Administration* (SOA). (Figure 1). Each buoy measured hourly wind data, surface currents, sea surface temperature, air temperature above sea level, and barometric pressure. Surface currents were recorded by a 1 MHz Nortek Aquadopp Current Meter with effective depth about 1 m (buoy A, B) and 4 m (buoy C). Both buoy A and buoy C collected data from 1 August to 1 September 2008 without temporal gap longer than 3 h. Valid data from buoy B started on 1 August, and ended on 20 August. Data gaps were filled with linear-temporal interpolation. Wind stress vector was calculated following *Smith* [1988] and wind velocity was corrected from 3.5 m (A, B) and 7 m (C) recorded height to 10 m standard height according to *Large and Pond* [1981].

### 2.4. Tide Gauge Records

[15] Hourly sea level records from tide gauges at Xiaomaidao station and Wuhaomatou station (Figure 1) were adjusted based on the same datum plane. Hourly sea level data used in this paper were from 1 August to 1 September, 2008. The inverse barometer effect was removed using atmospheric pressure observations from the meteorological station in Qingdao (for Wuhaomatou) and buoy A (for Xiaomaidao). A 48-h low-pass filter was performed to remove the tidal and inertial signals. Finally, the resulting time series were subsequently averaged to form daily sea level measurements. The daily sea level slope between Xiaomaidao station and Wuhaomatou station was defined as the barotropic pressure gradient between the inner bay and the outer seas.

## 3. Validation of Measurement

### 3.1. Radar Observations

[16] In order to assess the quality of HF radar currents, the differences and correlations between HF radar currents and those from three buoys were calculated on zonal ($U$) and meridional ($V$) components, respectively. The vector cross correlations were also evaluated according to *Kundu* [1976]. The closest HF radar grid points to each buoy were used. Results were summarized in Table 1. All individual component and vector cross correlations were significant (95% confidence level). At buoy A, the correlations of $U$, $V$ and vectors were highest, because its location nearly overlapped with the closest HF radar grids. The correlations of meridional components at buoy C were relatively low, most likely caused by its deeper effective measurement depth (4 m) and larger distance from the nearby HF radar girds. Phases of the complex correlation indicated that HF radar currents were clockwise rotating with respect to buoy currents at A and C, whereas counter-clockwise rotating at B.

[17] The root-mean square (RMS) difference between HF radar currents and buoy currents were also calculated

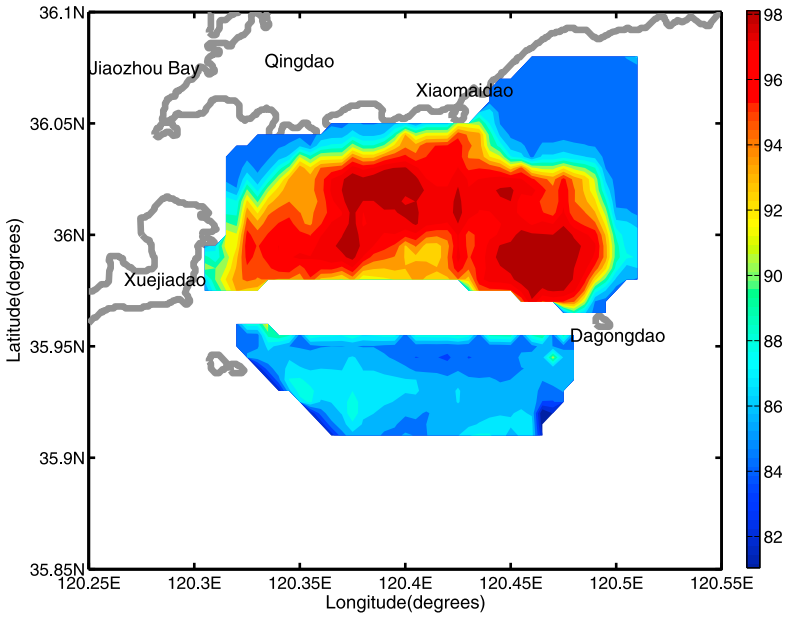


**Figure 2.** Percentage of temporal coverage of HF radar grid points.

(Table 1). The RMS difference for zonal component was generally larger than its meridional counterpart, since the alongshore currents were much stronger. It should be pointed out that three buoys and their corresponding nearest HF radar grid points did not completely spatially coincide. The nearshore currents might change dramatically within a small distance away. More importantly, HF radar currents were temporal-averaged over the sampling window and spatial-averaged along the radial direction at every radar grid point, buoy data, by contrast, was measured at a single point with sampling window only about 5 min.

[18] The above mentioned HF radar currents were derived using measured antenna beam pattern, which was believed to improve the accuracy of HF radar currents [*Paduan et al.* 2001; *Kohut and Glenn*, 2003]. To assess the improvement from the measured radar pattern, similar analysis was carried out with the currents from the ideal radar pattern (Table 1). At buoy B and C, both measured radar pattern and ideal radar pattern shared similar RMS difference and cross correlation with buoy currents. Although the measured radar pattern at buoy A slightly improved the comparison, HF radar currents from the measured radar pattern were used in this paper.

[19] The overall RMS difference (10 cm $s^{-1}$) was consistent with other comparisons between HF radar currents and meter currents [*Ebuchi et al.*, 2006; *Son et al.*, 2007] and HF radar-ADCP comparisons [*Kaplan et al.*, 2005; *Yoshikawa et al.*, 2007]. The significant statistical correlation and the reasonable RMS difference indicated that HF radar currents were reliable, and adequate to identify the key physical processes and dynamical features in this region.

### 3.2. Wind Data

[20] The temporal coverage and the locations of three buoys were compared. It is found that buoy A had least data

**Table 1.** Comparison Between HF Radar-Derived Currents and Buoy Currents[a]

| | Buoys | | | | | |
|---|---|---|---|---|---|---|
| | Buoy A | | Buoy B | | Buoy C | |
| HF Radar | Measured | Ideal | Measured | Ideal | Measured | Ideal |
| | | | *Zonal Component (U)* | | | |
| RMS difference (cm/s) | 11.3 | 12.5 | 9.9 | 9.8 | 12.1 | 12.0 |
| Correlation | 0.96 | 0.90 | 0.87 | 0.87 | 0.85 | 0.84 |
| Critical value (95%) | 0.39 | 0.41 | 0.32 | 0.32 | 0.38 | 0.37 |
| | | | *Meridional Component (V)* | | | |
| RMS difference (cm/s) | 10.6 | 11.5 | 9.9 | 9.6 | 11.5 | 11.6 |
| Correlation | 0.71 | 0.66 | 0.73 | 0.75 | 0.42 | 0.57 |
| Critical value (95%) | 0.34 | 0.41 | 0.38 | 0.37 | 0.35 | 0.33 |
| | | | *Complex Correlation* | | | |
| Magnitude | 0.93 | 0.84 | 0.85 | 0.86 | 0.77 | 0.80 |
| Critical value (95%) | 0.39 | 0.40 | 0.31 | 0.35 | 0.38 | 0.40 |
| Phase (deg) | −7.0 | −7.6 | 6.6 | 6.2 | −4.2 | 2.5 |
| Lower/upper limit, (deg) | −7.8/−6.2 | −8.0/−6.3 | 6.0/7.2 | 6.1/7.0 | −4.7/−3.5 | 1.5/3.7 |

[a]Measured, measured radar patterns; ideal, ideal radar patterns.

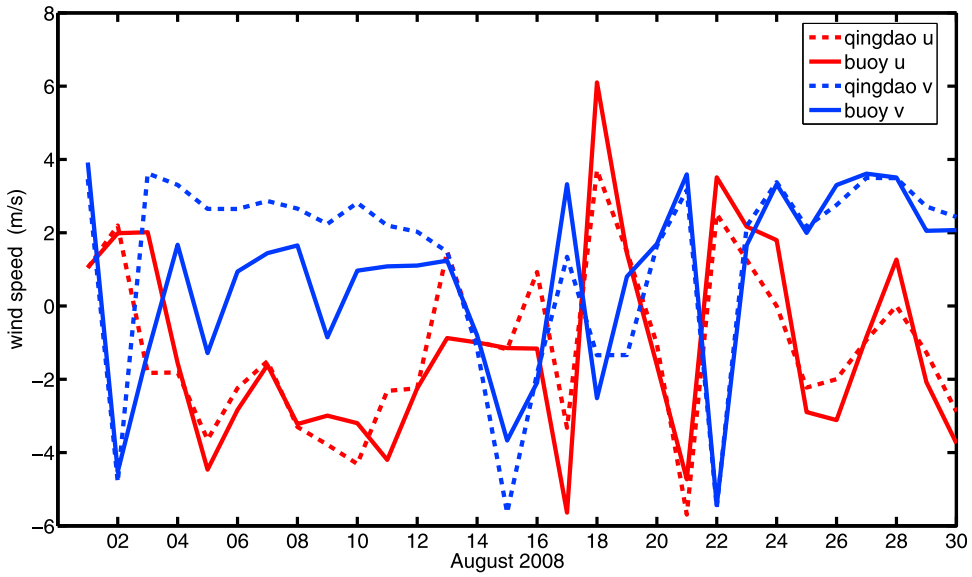


**Figure 3.** Wind measured by A buoy and Qingdao Baguanshan meteorological station. Solid red: buoy u; solid blue: buoy v; dashed red: Qingdao Baguanshan u; dashed blue: Qingdao Baguanshan v.

loss and its location almost remained unchanged. The wind data from buoy A was highly correlated with those from buoy B and C. The complex correlation between buoy A and B was 0.88 (angle, −7.46), and the correlation between buoy A and C was 0.84 (angle, 10.78). Thus, wind data from buoy A were preferred in this paper. In addition, the comparison between the wind records from buoy A and those from Qingdao Baguanshan meteorological station (Figure 1) revealed that both wind speeds were of the same order and covaried with time (Figure 3) with vector correlation 0.84 (angle, 9.43). Since buoy A and Baguanshan meteorological station are located at the center of Qingdao coastal sea, and they cover the majority of this region, it is reasonable to assume that wind field is uniform over the studied area. In this study, measurements from buoy A are regarded as the wind over the whole domain.

## 4. Characteristics of Currents Over Qingdao Coastal Sea

[21] Coastal currents are affected by many factors, such as tides, wind, pressure gradient, bathymetry, geometry as well as Coriolis effect. Different forcing mechanisms will drive the spatial variability at temporal scales from hourly to monthly. In this section, the coastal currents are decomposed according to their frequency and dynamically forcing factors.

### 4.1. Tidal Currents

[22] Tidal motions play an important role in the coastal dynamics of this region. Previous measurements and numerical model results revealed that barotropic semidiurnal tidal currents were dominant in Qingdao coastal waters [*Marine Environmental Monitoring Center*, 1992; *Chen et al.*, 1999; *Lozovatsky et al.*, 2008a; *Lu et al.*, 2008]. The snapshots of tidal currents pattern over a tidal cycle are derived from hourly HF radar currents (Figure 4). The surface currents, during flood tide (Figure 4a), are mostly southwestward, and veer southward to the east of Xuejiadao and westward at the entrance of the bay. This indicates that the tidal waves from Yellow Sea first arrive at the east edge of the radar region, and then rotate southwestward. When arriving at the mouth of Jiaozhou Bay, one branch propagates into the inner bay and modifies the inner bay circulation. The maximal surface current speed is about 100 cm $s^{-1}$. It is worth underlining that the surface tidal currents tend to align with the local isobaths and coastline.

[23] In contrast, surface flow, during an ebb tide (Figure 4c), is northeastward on the southern side of the domain, while deflected to eastward on the northern part. This behavior is expected for clockwise propagating tidal waves. The propagation of tidal wave is consistent with cotidal charts and previous numerical simulations [*Lee and Beardsley*, 1999; *Fang et al.*, 2004; *Xia et al.*, 2006]. Compared to the inflow during a flood, there is a notable outflow from the inner bay joining the ebbing currents. It is interesting to notice that the ebb tides from the inner bay and those of the outer waters do not completely overlap, as illustrated in Figure 4b. The outflow, disturbed by the currents from the southwestern part, becomes weak or even inverses to inflow near the bay mouth, giving rise to an asymmetric structure over a tidal cycle. This break in the ebb circulation is likely related to the seiches in Jiaozhou bay. Seiches in this region appear to be generated by the tides and local wind, and featured with high frequency oscillations. Their periods (about 2.3 h) are determined by the spatial dimension and mean water depth of the bay [*Lozovatsky et al.*, 2008a]. Seiches tend to be more obvious during the ebb tides because of the relatively weaker tidal velocities in this phase.

#### 4.1.1. Horizontal Distribution of Tidal Ellipses

[24] A harmonic tidal analysis was performed with T_tide toolbox [*Pawlowicz et al.*, 2002] to extract the tidal oscillations. Tidal ellipse parameters were calculated with 95% CI estimates. Resultant quantities were semi-major and semi-minor axes, ellipse orientations and phases, and were used to describe the tidal motions. Only harmonics with signal-to-noise larger than 10 was included in the following analysis.

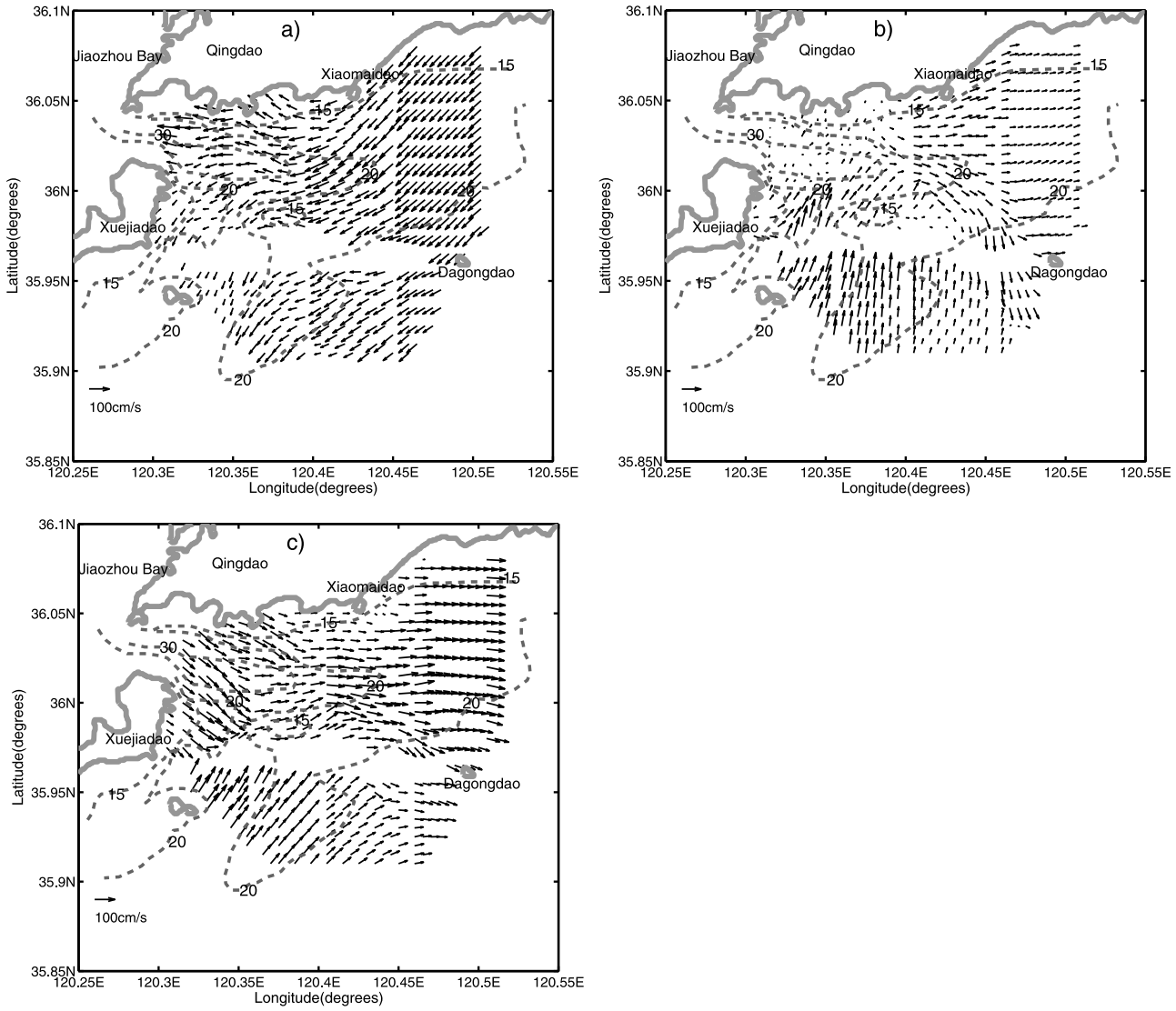


**Figure 4.** Snapshots of tidal currents over Qingdao coastal waters: (a) maximum flood, (b) initial ebb, and (c) maximum ebb. Dashed lines are isobaths in meters.

[25] Consistent with pervious observations [*Lozovatsky et al.*, 2008a; *Lü et al.*, 2008], semidiurnal tidal constituents are most pronounced. The distribution of the M2 and S2 tidal ellipses is shown in Figure 5. The M2 and S2 surface tidal orientations (angle between the semi-major axis and the east) are generally parallel to the local coastline; except the region near the entrance of the bay where orientations are steered by isobaths, demonstrating that the surface currents are strongly confined by the geometry and bathymetry. Phases of tidal ellipse (not shown), corresponding to the time at maximum current, suggest the counterclockwise propagation of tidal waves during flood tides.

[26] The deep channel connecting the inner bay and the open waters divides the study area into two distinct parts (line A in Figure 5). The tidal ellipses between the two parts are striking different. First of all, the surface tidal ellipses are differently polarized. Eccentricity on the left-hand side (larger than 0.4) are much larger than those of the right-hand side (with the order of 0.1), reflecting different types of tidal currents between them. Surface currents will rotate dramatically during a tidal cycle over the left-side region where the topography is nearly flat. In the right-side part, nevertheless, the variations of geometry and topography result in rectilinear currents. Another feature that distinguishes them is their different rotating directions. Tidal currents are counterclockwise rotating on the left of line A, while clockwise rotating on the right. It is worthy noting that the tidal ellipses are strongly eccentric on the right side, which makes it not safe to determine the clockwise rotating direction. During the tidal ellipses analysis, the ratio of the counterclockwise rotation amplitude to the clockwise one is about 0.7 on the right side, and suggesting that clockwise rotating is more pronounced. It is also found that consistent clockwise rotation also present in the currents from buoy A, B, and C, thus, supporting the robust of HF radar currents. However, different rotating directions are shown in ADP currents measured in May (Table 2). It is presumable that the clockwise rotation is the leakage from the sub-tidal

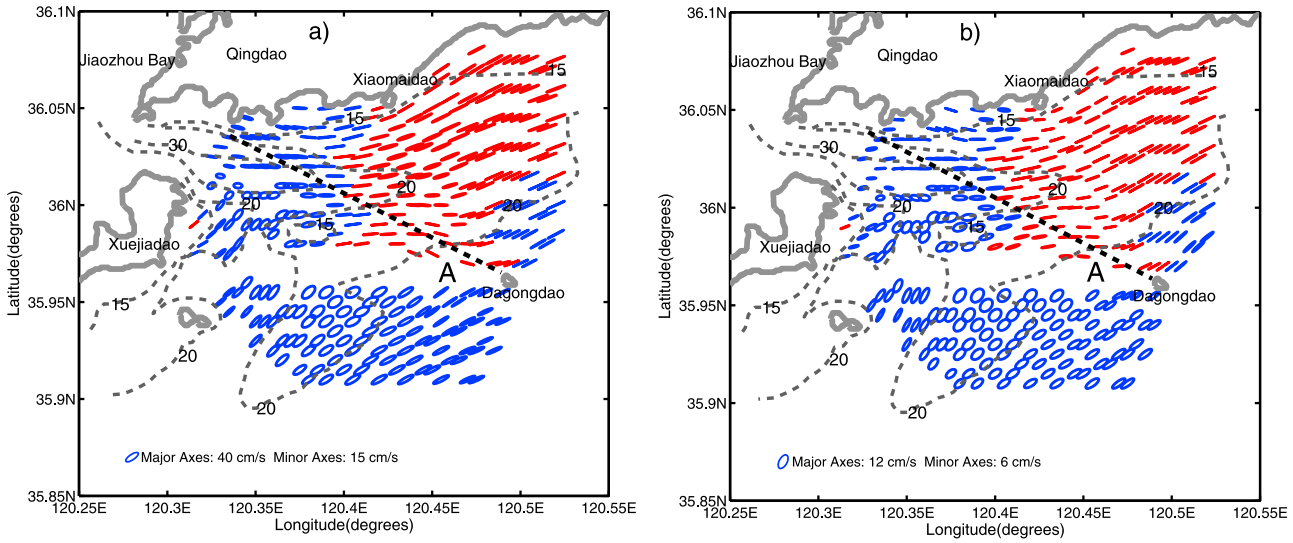


**Figure 5.** Tidal ellipses for (a) M2 and (b) S2 tide constitute surface tidal currents. Blue denotes counter-clockwise rotation, red denotes clockwise rotation. Dashed gray lines are isobaths in meters. Dashed thick black line is parallel to the deep channel near the entrance of Jiaozhou Bay.

currents during August. Due to the opposite signs of rotation, local surface divergence (convergence) is found during some periods of tidal cycles (not shown).

[27] Finally, tidal current amplitudes also show an obviously dissimilar distribution. The amplitudes of the M2 constituent reach 0.6 m $s^{-1}$ in the vicinity of Xiaomaidao Island, and decrease rapidly to 0.1–0.15 m $s^{-1}$ when moving toward the southwestern part of the coverage area. This can be explained by the different water depths of the two parts. In particular, the right part is generally shallower than the left, and strong tidal current tends to occur in the shallow waters. Please note that, the minimum tidal currents take place near the bay mouth where a deep trench lies. Out of the northwestern edge of the radar coverage, according to historic observations and numerical results [*Editorial Board of Annals of Bays in China*, 1993; *Lü et al.*, 2008], the M2 tidal amplitude will intensify rapidly when moving toward the inner bay due to the impact of both water depth and complicated geometry.

### 4.1.2. The Vertical Distribution of Tidal Ellipses

[28] An identical tidal analysis was performed on moored ADP data. The ellipse parameters for the M2 and S2 tidal constituents at the mooring D site (Figure 1) are given in Table 2. The major axes of M2 component are similar throughout the water column. Over the upper 4.9 m, the maximal tidal current is 20.9 cm $s^{-1}$ and decreases to 20.3 cm $s^{-1}$ and 20 cm $s^{-1}$ at 6.6 m and 8.3 m, respectively. The minor axes are about 0.5–1% of the major axes, but with greater uncertainty compared to major axes. The ellipses are oriented in the alongshore direction, pointing to the rectilinear motions in alongshore direction, which is consistent with HF radar currents in summer. In addition, both phases and inclination angles for the M2 tidal current were quite uniform throughout the water column, suggesting a barotropic M2 tidal flow. The S2 constituent shares similar characteristic with M2 constituent, but their major axes are only about 8–9 cm $s^{-1}$, much smaller than the M2 constituent. Consequently, their minor axes are more erratic, and lead to erratic inclinations and phase differences. These minor axes are normal to the local isobaths, and may be largely influenced by the frictional boundary layers.

[29] Generally, hourly HF radar currents analysis successfully describes the local surface circulation over a tidal cycle. The horizontal and vertical distribution of the tidal

**Table 2.** Result From Harmonic Analysis of ADP Currents[a]

| | M2 | | | | S2 | | | |
|---|---|---|---|---|---|---|---|---|
| Depth (m) | Major (cm/s) | Minor (cm/s) | Inclination (deg) | Phase (deg) | Major (cm/s) | Minor (cm/s) | Inclination (deg) | Phase (deg) |
| 3.2 | 20.9 | 0.3 | 0.4 | 286.5 | 9.5 | 0.1 | 179.0 | 146.8 |
| 4.9 | 20.9 | 0.2 | 179.3 | 105.5 | 9.1 | −0.1 | 178.9 | 151.4 |
| 6.6 | 20.3 | 0.1 | 179.1 | 103.8 | 9.7 | −0.1 | 179.5 | 149.7 |
| 8.3 | 20.0 | −0.1 | 179.5 | 104.6 | 9.2 | −0.3 | 178.9 | 146.7 |
| 10.0 | 20.6 | 0.1 | 178.8 | 106.4 | 8.7 | 0.1 | 0.3 | 327.9 |
| 11.7 | 20.4 | 0.2 | 179.2 | 107.8 | 8.6 | 0.1 | 178.3 | 151.2 |
| 13.4 | 19.1 | 0.1 | 178.6 | 107.0 | 8.9 | 0.1 | 179.1 | 144.7 |
| 15.1 | 18.6 | 0.1 | 179.6 | 107.1 | 7.1 | 0.3 | 178.9 | 151.4 |
| 16.8 | 18.0 | −0.3 | 179.9 | 105.3 | 8.3 | −0.1 | 2.0 | 331.0 |

[a]Negative in minor reflects clockwise rotation while positive for counter-clockwise.

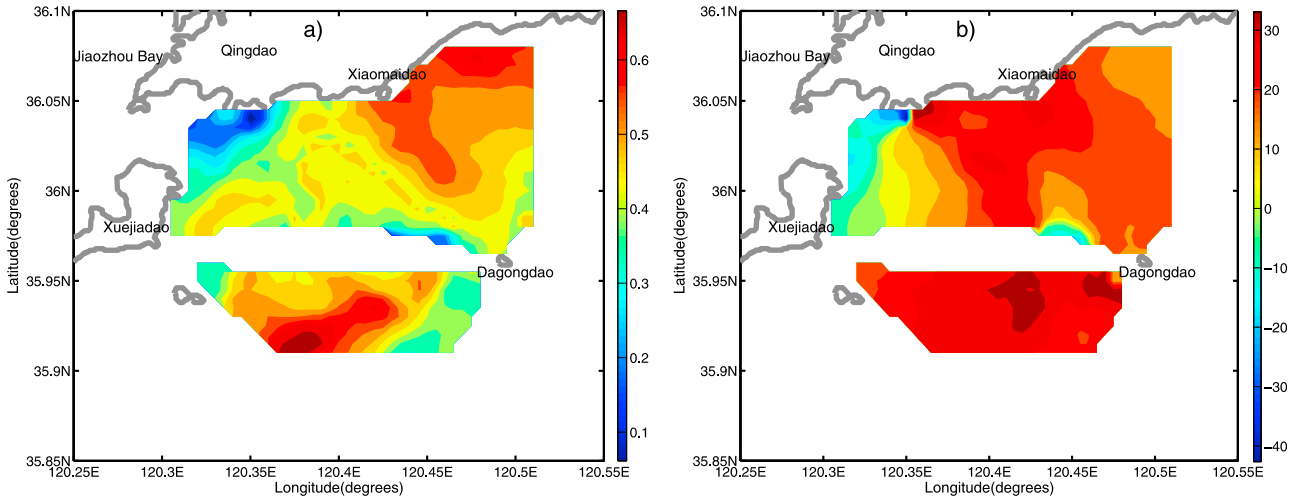


**Figure 6.** Cross correlations between sub-tidal currents and wind data from A buoy. Sub-tidal currents were derived from HF radar currents. (a) Magnitude and (b) phase (in degrees) of complex correlation between sub-tidal currents and wind from A buoy. Positive phase indicated that sub-tidal current, clockwise rotated with respect to wind data.

ellipses reveals the remarkable influence of geometry and topography on sea surface tidal currents. These observations can be used as calibration and independent comparison for the dynamical structure of numerical simulations in the future.

### 4.2. Wind Driven Currents

[30] In Qingdao coastal waters, the local wind is a dominant source of sub-tidal variability for sea surface currents. Complex correlations between the sub-tidal currents and the wind data at buoy A are calculated to better understand the coherence between them. The sub-tidal currents are derived from HF radar currents and the buoy currents by applying a 48-h low-pass filter to remove all tidal and inertial fluctuations. A lagged complex correlation is calculated between the filtered buoy currents and wind. Results exhibit that the maximum correlation occurs when the wind lead currents about 9 to 10 h, suggesting that it takes 9–10 h to establish an equilibrium of wind-driven response. This time scale corresponds to half of the inertial period (about 19 h) and is consistent with previous studies [*Zhao*, 1982; *Yoshikawa et al.*, 2007]. The correlations between the filtered HF radar currents and wind with wind leading 9 h are shown in Figure 6. In general, the obtained correlations are greater than 0.45 over the majority of the radar coverage with 95% confidential level of 0.34 (Figure 6a). In the northwestern part, by contrast, complex correlations are much lower, reflecting that wind-driven currents might not predominating in that local area (section 5). Another low correlation region is close to the discontinuity area, presumably due to the poor data quality there. Phases of the complex correlations (Figure 6b) indicate that the HF radar variability is rotated about 10°–30° clockwise relative to winds. The angles appear to be more uniform except the two regions where high correlations breakdown. Given constant vertical eddy viscosity and infinite depth, the simple Ekman theory predicts that the surface currents are 45° clockwise deflected with respect to wind. However, the water depth in the coastal region is usually comparable to the Ekman depth. The depth of the surface Ekman layer can be estimated [*Csanady*, 1976; *Lentz*, 2001] for an unstratified water column:

$$h = \frac{\kappa}{f}\sqrt{\frac{\tau_s}{\rho}},$$

where $\kappa = 0.4$ is the von Karman constant, $f$ is the Coriolis parameter, and $\rho$ is the water density, and $\tau_s$ is the surface wind stress. If the wind stress is derived from monthly mean wind, then $h = 45\ m$. In Qingdao coastal water, the mean water depth is about 15 m, leading to a ratio of $h$ to the total water depth about 3:1. According to *Ye and Li* [1991], the angle between wind and the surface currents should be about 30°, consistent with phases in Figure 6b. In addition, the energy transfer between the local wind and the surface currents, defined as the ratio of the surface sub-tidal currents speed to wind speed, is about 1%–3%, and considerably agree with the continuity of the momentum flux through the air-sea interface [*Kudryavtsev et al.*, 2008].

[31] The HF radar currents provide valuable fine-scale illustrations of the surface currents over a large region. To further examine the detailed response of the surface current to local wind, the spatial pattern of daily averaged sub-tidal flow during several wind events are studied. It can be seen that several episodes of strong wind incidents represent the different weather conditions during August 2008 (Figure 7). Two sustained incidents are selected, but separated into three according to different wind directions: varying wind from 17 August (southeasterly) to 18 August (northwesterly), and the northerly wind on 31 August. The reference time is local time (120° E time zone).

[32] Strong wind episodes start at 0400 on 17 August, end at 1300 on 18 August, with peak winds of 11.5 m $s^{-1}$. During this period, the wind directions reverse from the southeasterly on 17 August (between 0400 and 2400) to the northwesterly on 18 August (Figure 7). To better understand the effect of the local wind on 17 August, the surface currents on 16 August are also examined. The local wind is

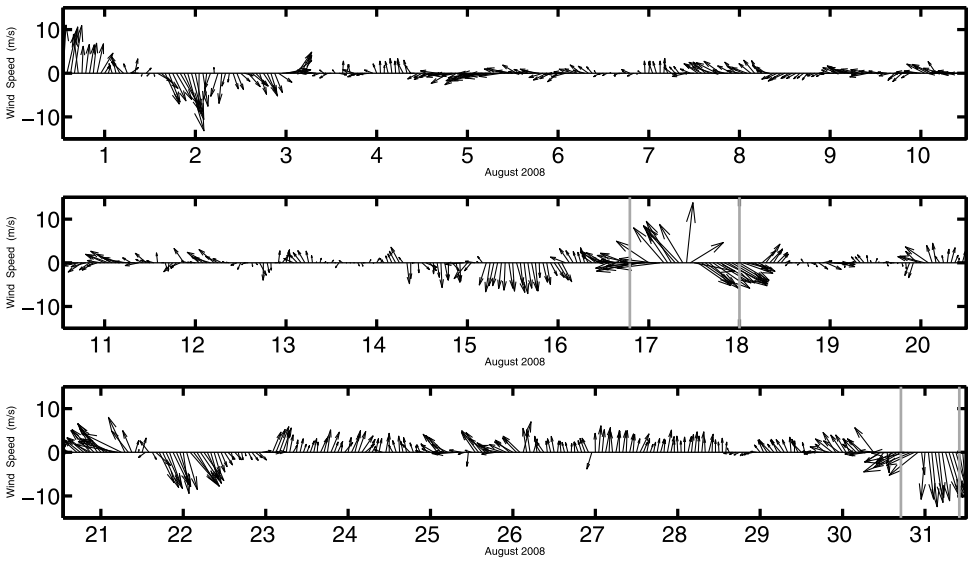


**Figure 7.** Wind vector measured by buoy A. Three wind incidents (17 August, 18 August and 31 August) are marked by a gray solid line.

weak northwesterly on 16 August, and the daily surface sub-tidal currents are shown in Figure 8a. A branch outflow from Jiaozhou Bay (section 5) is observed by the HF radar. To the south of Xiaomaidao, one branch of outflow is directed nearly along local isobaths, producing a coastal jet. The southwestward flow on the south of 35.95°N is not likely related to wind, because their ratio to local wind exceeds 6%. On the contrary, the local wind becomes strong southeasterly on 17 August, the surface currents to the south of 35.95°N, driven by wind, flow onshore (Figure 8b), forming the local convergence immediately north of 35.95°N. Both the outflow and the coastal jet south of Xiaomaidao are weaker than previous day, indicating that this costal jet was closely related to the outflow of Jiaozhou Bay.

[33] When the wind direction reversed quickly to northwesterly on 18 August, the surface sub-tidal current field exhibits more complicated structure (Figure 8c). The surface currents in the southern part (open waters) turn westward, but still toward Xuejiadao. There is interesting fine scale circulation (about 5 km) south of Xiaomaidao, and might be steered by the local 20 m isobath. Another sub-mesoscale eddy develops to the east of Xuejiadao and near the entrance of Jiaozhou Bay, modifying the local coastal circulation. Although this eddy is temporal, it is very close to the Olympic sailing race venue, where the variability of the surface current structures should be taken on greater importance. It is noticeable that the outflow of Jiaozhou Bay is replaced by a strong inflow, probably induced by the sub-mesocale eddy.

[34] The sub-tidal currents on 31 August clearly demonstrate the crucial impact of the local wind-forcing. Strong northerly winds prevail from 31 August 0300 to 2300 (local time). The surface current field becomes more coherent. The outflow from Jiaozhou Bay joins the wind-driven current and flows southward with the maximum speed of 53 cm $s^{-1}$ (Figure 8d). Note that, the order of sub-tidal currents is comparable to the tidal components, and flows over the open waters are generally stronger than the nearshore. Under the control of wind, the coastal jet along the south of Xiaomaidao also reverses. The mean angle between the wind and the surface sub-tidal currents are about 40°, as expected from the surface Ekman dynamics.

### 4.3. The Monthly Averaged Currents

[35] The low-pass filtered radar currents are averaged over the entire month to investigate the relative steady coastal surface circulation. A strong outflow from Jiaozhou Bay is observed in the northwestern part of the region with speed up to 0.2 m $s^{-1}$. The outflow appears to follow the local coastline, then splits with one part flowing southward and the other continuing eastward and then turning southward near 120.45°E. The first part turns southward and strengthens, finally generates an evident clockwise eddy pattern with the core overlapped with the local isobath (Figure 9). On the monthly scale, the averaged circulation is geostrophic. According to the barotropic potential vorticity theory, the surface currents in this shallow region tend to be steered by isobaths. A similar sub-mesocale eddy structure is also resolved by numerical modeling forced by tides only [*Chen et al.*, 1999; *Yan et al.*, 2001; *Lü et al.*, 2008]. Thus, this eddy structure circulation more likely results from the tides and bathymetry rather than wind. If the monthly averaged currents are considered as the coastal circulation during August 2008, this spatial pattern is found by the observations for the first time. Due to the existence of a clockwise eddy in monthly coastal currents, the materials and pollution carried by the residual currents might be potentially transported to the northeastern part of the HF radar coverage. An additional feature is that these monthly residual currents are closely related to the outflow near the entrance of Jiaozhou Bay, where the wind-driven currents is not dominant. In the next section, the surface dynamics in that local area will be further explored.

## 5. The Momentum Balance at the Entrance of Jiaozhou Bay

[36] Velocities normal to the section (dashed line in Figure 9) near the Jiaozhou Bay mouth are shown in Figure 10. In

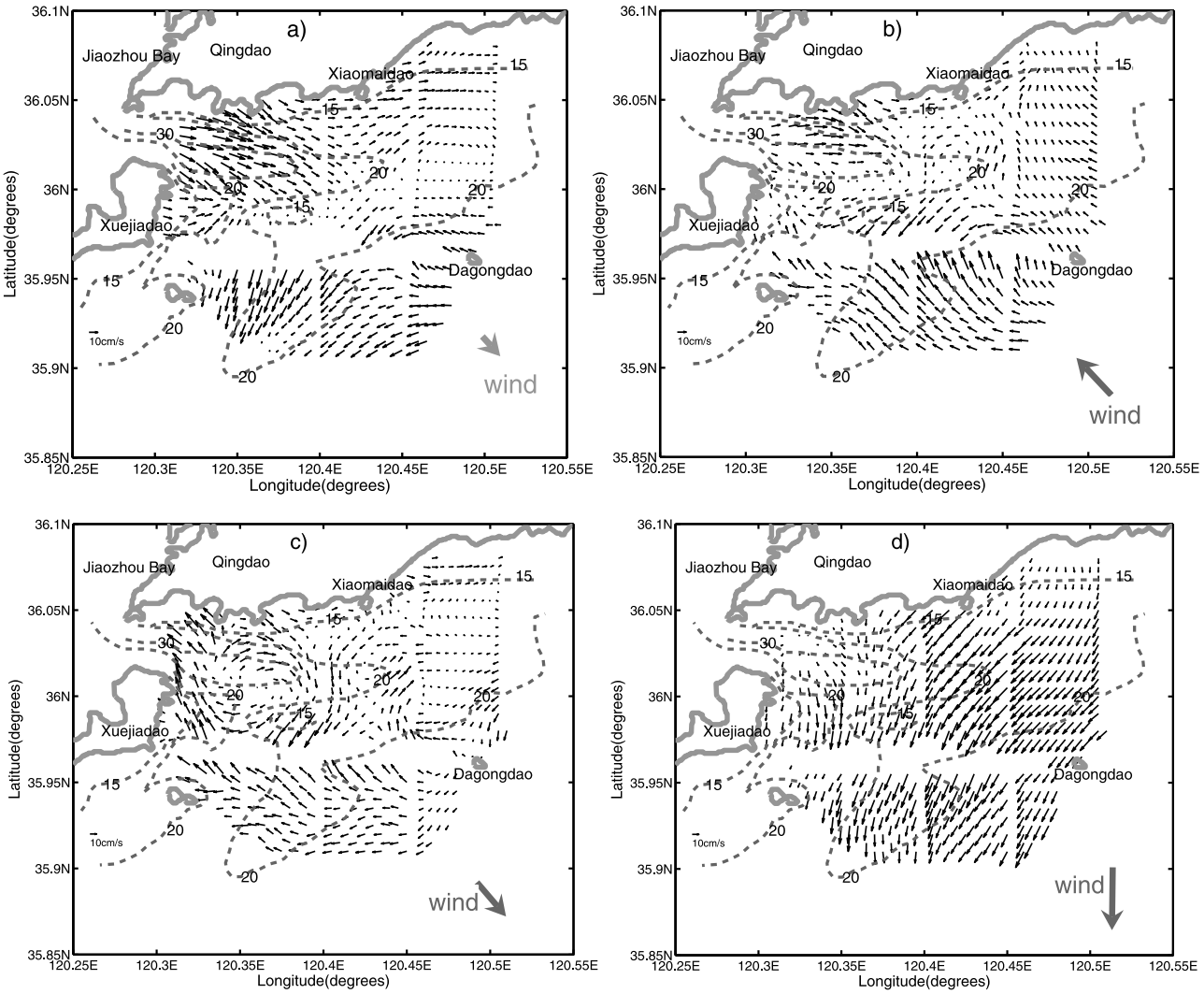


**Figure 8.** Surface sub-tidal currents during wind incidents (a) under weak northwesterly wind on 16 August, (b) under northeasterly wind on 17 August, (c) under northwesterly wind on 18 August, and (d) under northerly wind on 31 August. Shaded arrows indicate the wind speed and direction from A buoy. Dashed lines are isobaths in meters.

August 2008, there is an outflow in the northern part of the section and an inflow in the southern part. The opposite direction of the flow along the section confirms the existence of a counterclockwise eddy in Figure 9. This eddy structure disappears temporally in mid-August, and then intensifies later this month. Its variability tend to change the water discharge between the inner bay and the outer waters, thus it is desirable to quantify the factors that modulate its fluctuations by analysis of the momentum equation near the entrance of Jiaozhou Bay. The momentum equations are

$$\frac{du}{dt} - fv = -\frac{1}{\rho_0}\frac{\partial P}{\partial x} + A_z\frac{\partial^2 u}{\partial z^2} \tag{1}$$

$$\frac{dv}{dt} + fu = -\frac{1}{\rho_0}\frac{\partial P}{\partial y} + A_z\frac{\partial^2 v}{\partial z^2} \tag{2}$$

[37] Here the lateral friction is neglected. The velocities ($u$, $v$) are decomposed into sub-tidal components ($U$, $V$) and tidal components ($u'$, $v'$). The surface stress is wind stress ($\tau_{wx}$, $\tau_{wy}$). The surface (upper 1 m) momentum balances in the $x$ (zonal) and $y$ (meridional) directions are written as

$$-fV = -\frac{1}{\rho_0}\int_{-1}^{0}\frac{\partial P}{\partial x}dz + \frac{\tau_{wx}}{\rho_0} - \left\langle u'\frac{\partial u'}{\partial x} + v'\frac{\partial u'}{\partial y}\right\rangle \tag{3}$$

$$fU = -\frac{1}{\rho_0}\int_{-1}^{0}\frac{\partial P}{\partial y}dz + \frac{\tau_{wy}}{\rho_0} - \left\langle u'\frac{\partial v'}{\partial x} + v'\frac{\partial v'}{\partial y}\right\rangle \tag{4}$$

[38] Over daily timescale of interest here, the local accelerations and nonlinear advection terms of the sub-tidal currents have been neglected. $P$ is pressure, $f$ is the Coriolis parameter, $\rho_0$ is the reference density, and $\langle\ \rangle$ represents a tidal average. The last two terms on the right-hand side of equations (3) and (4) are advective tidal stresses [*Visser et al.*, 1990], which are the contribution of tidal energy to

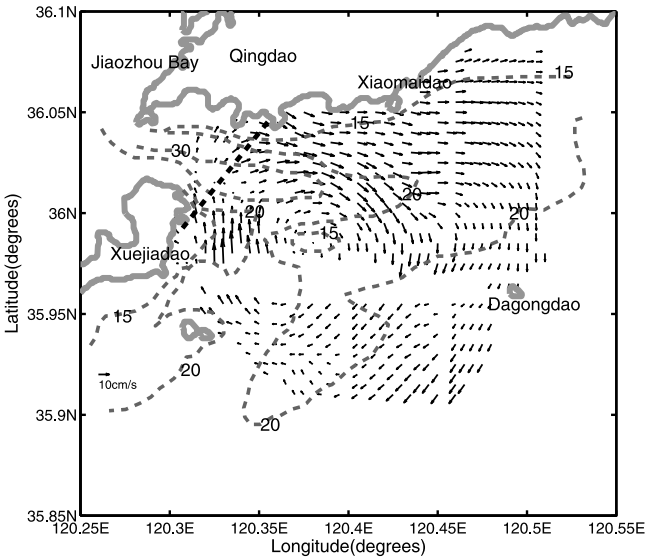


**Figure 9.** Monthly residual currents during August 2008. Dashed gray lines are isobaths in meters. Dashed thick black line across the entrance of Jiaozhou Bay is the section used for momentum balance analysis.

the sub-tidal flow. Here only lateral tidal stress is used, since vertical shear is negligible.

[39] Equations (3) and (4) are projected to the along-shore direction (normal to the section in Figure 9) and the cross-shore direction, with the along-shore component is defined to be clockwise rotating 45° from the east, which is roughly parallel to the local coastline. Only the momentum in cross-shore direction is analyzed here. The Coriolis term is estimated by averaging measured HF radar currents in along-shore direction and can be taken as the variability of net velocity in the section. The wind stress is computed using instantaneous wind observations from buoy A, then low-pass filtered and daily averaged. The tidal parameters obtained from harmonic analysis of HF radar currents are used to reproduce the tidal currents in this area, and then derive the lateral tidal stresses. Near the mouth of Jiaozhou Bay, the tidal currents are highly asymmetric over a tidal cycle, In particular, the ebb currents are generally smaller than the flood currents but the ebb period (about 6.8 h) is longer than the flood period (about 5.6 h). Figure 11 illustrates the asymmetric structure over several tidal cycles on the section, with alternative inflow and outflow during flood and ebb, respectively. The gray diamond marks the transitory disturbance over a tidal cycle. Similar signals were also observed by *Lozovatsky et al.* [2008a], and were attributed to the interaction between seiches generated inside the bay and the barotropic tides. This asymmetric flow over a tidal cycle should contribute to the tidal stresses.

[40] Qingdao coastal sea level has clear annual variability [*Editorial Board of Annals of Bays in China*, 1993; *Pu et al.*, 2004], with ascending cycles from February, peak in August and then descending cycles from September to the following February. But the sea level over this coastal region is not uniform. Due to the local wind, geometry, and runoff from rivers around Jiaozhou Bay, there will be sea level difference between the inner bay and the outer seas. Two tidal gauge stations, Xiaomaidao station and Wuhaomatou station, are selected to represent the sea level of the inner Bay and the outer waters, respectively (Figure 1). The sea level slope between the inner bay and the outer bay is used to estimate pressure gradient, i.e., the first term of the right hand side of equations (3) and (4).

[41] Each term of the momentum equation in cross-shore direction is shown in Figure 12. It is obvious that the surface momentum equation is predominately balanced by the barotropic pressure gradient, the Coriolis term and the tidal stress. The sea level of the inner bay is generally higher than the outside, which produces pressure gradient (only cross-shore pressure gradient is used). The barotropic pressure

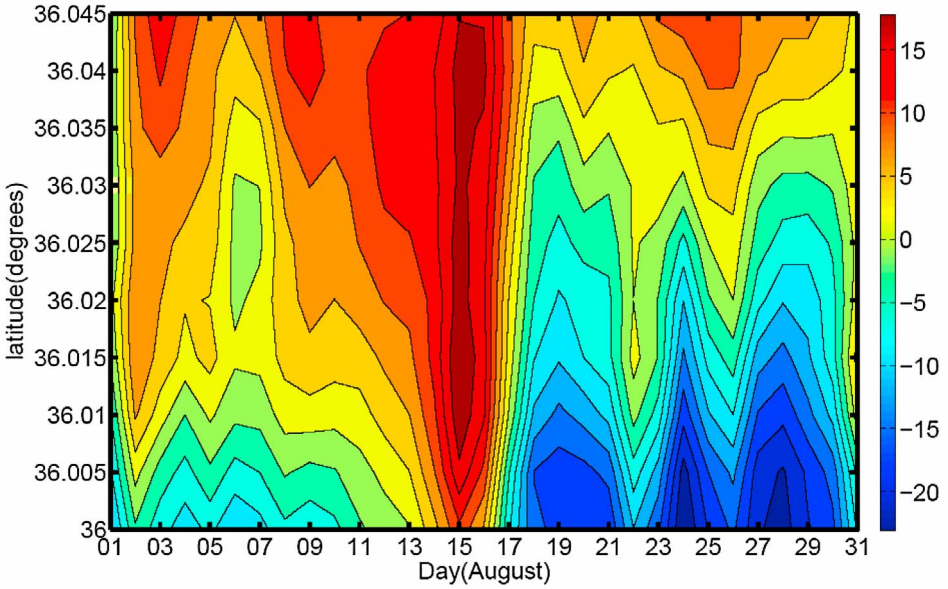


**Figure 10.** Sub-tidal velocities (cm/s) normal to the section near the mouth of Jiaozhou Bay. Positive: outflow; negative: inflow.

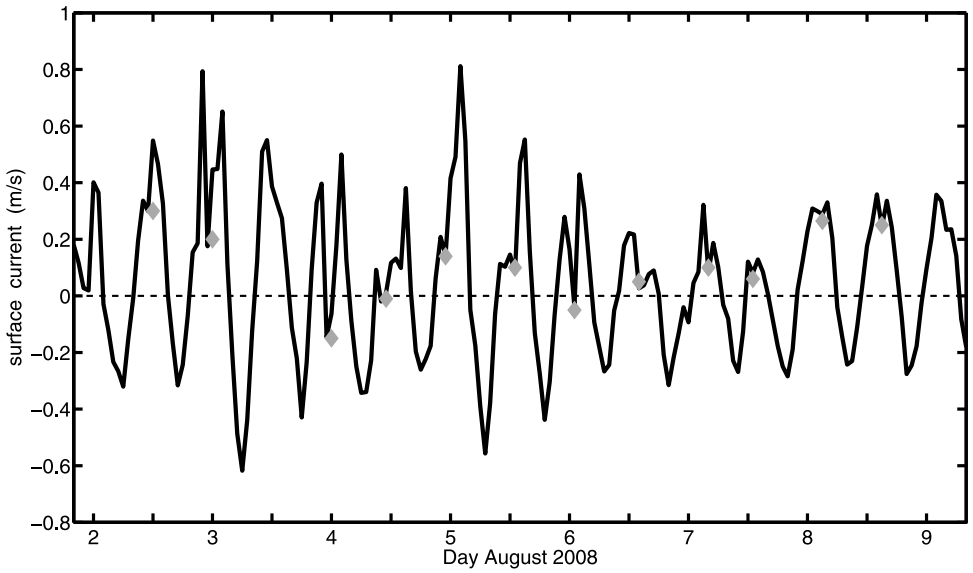


**Figure 11.** Surface currents over tidal cycles on the section across the mouth of Jiaozhou Bay. The section is shown in Figure 9. Positive value means outflow (ebb current); negative value is inflow (flood currents).

gradient tends to drive an outflow during August and the outflow further results in eddy structure circulation in the monthly coastal circulation (Figure 9). The magnitude of wind is much lower, except during several strong wind events. The wind directions are normal to the section during 17–18 August; thus have notable effect on the momentum equation. The tidal stresses (yellow bar in Figure 12) varied with time. During the spring tide (Mid-August), tidal stresses together with the barotropic pressure gradient drive an outflow. The strong inflow brought by the tidal stresses during the neap tide (around 5 August and 21 August), however, counter to the outflow driven by the pressure gradient. Interestingly, the variability of tidal stresses is much larger than the pressure gradient, and is able to temporally modify the circulation near the entrance of Jiaozhou Bay. Figure 12 shows that both the pressure gradient and the tidal stresses determine the fluctuations of the net velocities. That is to say, the evolution of the eddy structure in the monthly coastal

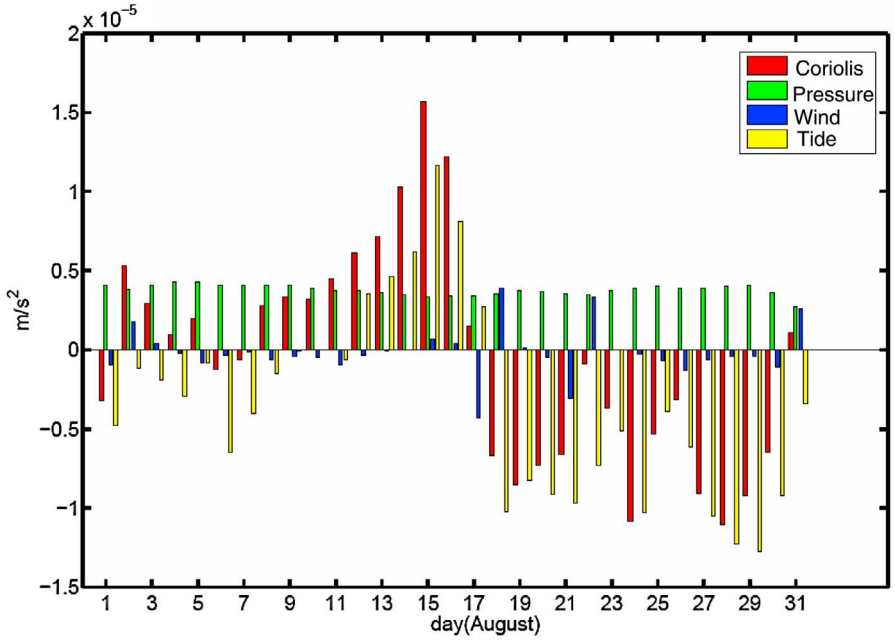


**Figure 12.** Terms of the momentum equation in alongshore direction. Their values are illustrated by color bars. Red: Coriolis term (from HF radar observations); green: barotropic pressure gradient (from sea level difference); blue: wind stress (from A buoy measurements); yellow: tidal stress (from repredicted tidal currents).

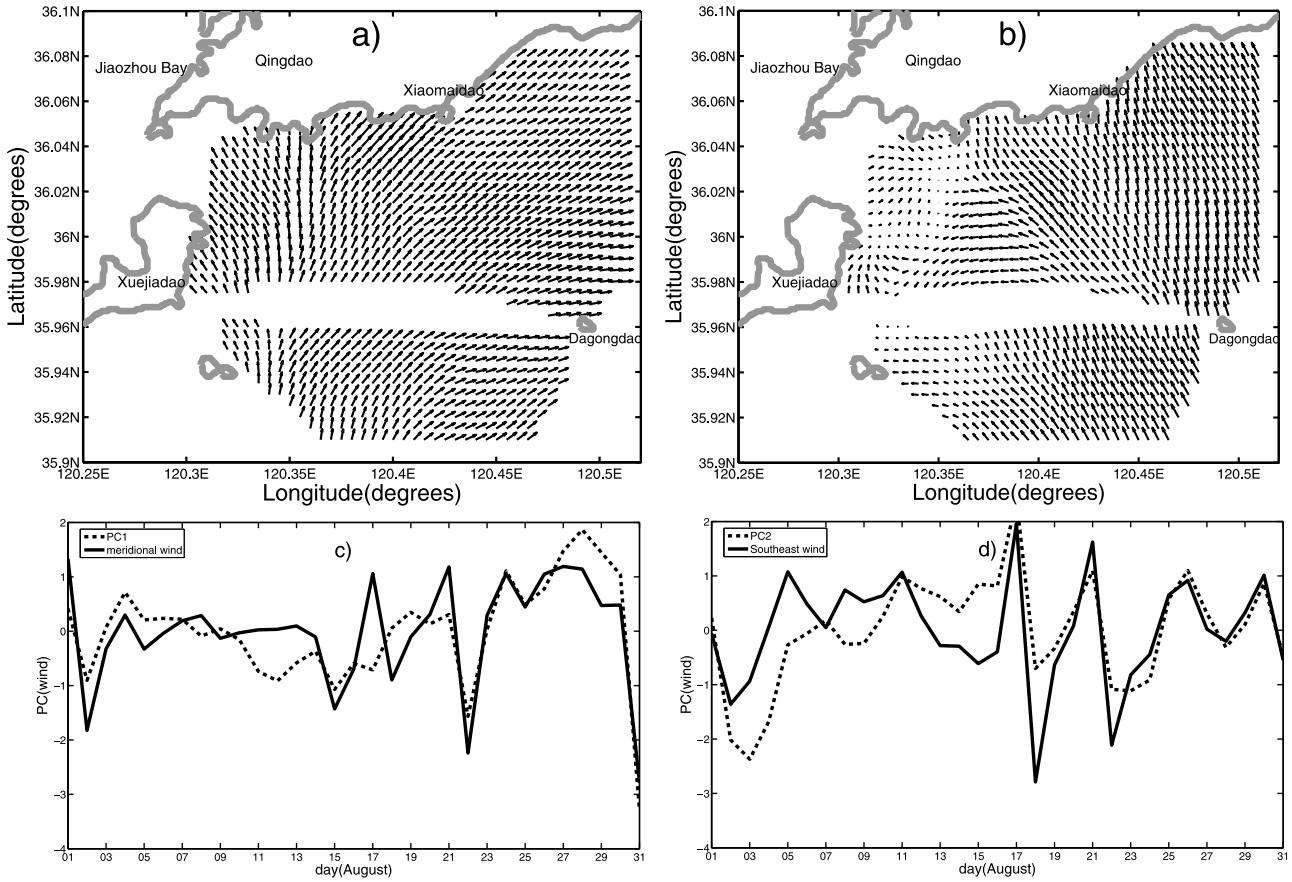


**Figure 13.** Empirical orthogonal functions (EOF) of sub-tidal current data: the spatial pattern of (a) mode 1 and (b) mode 2 and the time series of the (c) first and (d) second EOF mode. In order to compare, EOFs are all normalized to have unit magnitude.

circulation is mainly governed by the tidal stresses and the pressure gradient (sea level slope). It should be emphasized that the estimation about tidal stress is only based on the lateral tidal stress $\left\langle u'\frac{\partial u'}{\partial x}+v'\frac{\partial u'}{\partial y}\right\rangle$, and assume other forms of tidal stresses are negligible. The phases of the tidal stress between 1st August and 17 August are consistent with the spring-neap cycle. After that, the negative stresses lasting about 2 weeks seems deviate from the spring-neap cycle, which should shift to positive around 26 August. Because the surface tidal currents are not available during September, it is still unclear why the last few days have irregular changes. We speculate that it might result from the seasonal transition or other lower frequency signals. Nevertheless, the analysis about the momentum balance qualitatively highlights the significant role of the nonlinear tidal stress and the nearshore sea level slope in this coast region. More attention should be paid to them when studying the coastal dynamics and the material transport over coastal waters of Qingdao.

## 6. Discussion and Summary

[42] New observations from HF radar and ADP have been used to examine the time-varying spatial structure of the coastal currents around Qingdao nearshore waters. The tidal motions are most energetic and dominate the semidiurnal and diurnal variability. Particularly, an analysis about the tidal ellipse shows that the variations of the surface tidal currents during flood and ebb periods are determined by tidal waves, geometry, and bathymetry. For example, in shallow waters, isobaths steer surface currents, and the steep topographic gradient even lead to rectilinear currents. Surface currents in deeper waters, however, are mainly influenced by tidal waves and exhibit rotating features. This is also the reason that the local bathymetry and geometry divide the HF radar coverage into two distinct regions. The two regions are separated by different rotations, eccentricity, and different amplitudes of the ellipses. In fact, two types of the tidal flow (reversing tidal current and rotating current) produce different near-bottom dissipation rates and friction velocities [*Lozovatsky et al.*, 2008b]. Our analysis, for the first time, describes the spatial distribution of these two typical flows. The harmonic analysis with ADP currents is consistent with HF radar currents and previous in situ observations, but further demonstrates the barotropical structure over the water column.

[43] Over the inertial frequency, the impact of wind is significant, especially over the open waters. Both the local wind stress and the tides contribute to the local sub-mesoscale circulation, which is crucial for the near-surface convergence (divergence) and water transport. To better understand the spatially coherent variations between the local wind and sea surface currents, an EOF analysis is performed on sub-tidal

currents. The first mode explains 62.3% of the overall variance, and represents the surface currents driven by meridional wind (Figures 13a and 13c). Correlation between the first EOF mode and the normalized meridional wind is significant (0.74) at 95% confidence level (0.62). Under the control of the meridional wind, the surface current flow clockwise toward the northeastern part of the HF radar coverage. An important feature is that a branch of the wind-driven flow is deflected into Jiaozhou Bay, revealing the contribution of wind to the seiches of Jiaozhou Bay [*Lozovatsky et al.*, 2008a], the annul cycle of sea level in the Bay [*Pu et al.*, 2004], and the spatial distribution of nutrients in this area [*Chen et al.*, 1999].

[44] The second EOF mode accounts for 21.5% of the variance and reflects the pattern forced by the southeasterly wind (Figures 13b and 13d). The temporal amplitudes of the second EOF mode show a coherent variation with the normalized southeasterly wind (correlation, 0.63). The horizontal pattern is dominated by onshore flow, but near the entrance of the bay the sea surface currents are quite weak.

[45] In Qingdao coastal waters, if the complicated coastline is also taken into consideration, wind directions should not be ignored. The first and the second EOF modes represent different patterns driven by different local winds. In open waters, the surface currents tend to follow the wind direction, but they appear to show different distribution when moving toward nearshore, especially over the waters near the bay mouth. The analysis of the daily averaged subtidal flow during several wind incidents also indicates the influence of wind direction on the generation of the submesoscale circulation.

[46] In addition, new observations about the monthly residual currents exhibit the detailed structure about the coastal circulation. In summer, there is an outflow from Jiaozhou Bay, and might transport nutrients and pollution out of the bay, which is the fundamental process of the self-purification of Jiaozhou Bay. The outflow is then controlled by the barotropic vorticity in shallow waters and generates an eddy circulation. The clockwise eddy structure circulation is the dominating feature in Qingdao coastal circulation in August.

[47] Further examination about the cross-shore surface momentum balance near the entrance of the bay suggests that the monthly outflow is resulted from the interplay between the barotropic pressure gradient and the tidal stresses. The sea level difference between the inner bay and the outer waters generates pressure gradient across the bay, further inducing an outflow in August. On the other hand, the nonlinear tidal stresses transfer energy from tidal motions to monthly circulation, corresponding to the tidal induced residual circulation. It is found that the variance of tidal stresses during August is remarkably related to the variability of the outflow. For example, the outflow reverses during mid-August when tidal stresses shift phase (Figure 10).

[48] New understanding about the nearshore dynamics in Qingdao coastal waters and Jiaozhou Bay will help to determine the crucial location for following in situ experiments. On the other hand, the new measurement should shed a light on the improvement of numerical modeling. In particular, a new forecasting system assimilating the HF radar currents is under construction. It is believed that the HF radar systems will speed up the development of operational oceanography in this area and promote the preservation, management, and sustainable development of Jiaozhou Bay.

[49] **Acknowledgments.** This study was supported by the National High Technology Research and Development Program of China (863 Program) (2007AA09Z117), BMBF project CHN 09/031 and National Department Public Benefit Research Foundation (Oceanography, 200805006). We also thank X. W. Bao and S. H. Gao for providing the ADP measurement and wind observations. The authors are grateful to two anonymous reviewers for their insightful comments, which led to a greatly improved manuscript.

## References

Bao, X., J. Yan, L. Zhao, and L. Shi (1999), Application of ECOM to simulate tidal currents in Jiaozhou Bay (in Chinese), *Mar. Sci.*, *5*, 57–60.

Barrick, D. E., and B. J. Lipa (1996), Phase 1 SBIR final report: Comparison of direction-finding and beam-forming in HF radar ocean surface current mapping, technical report, NOAA, Rockville, Md.

Barrick, D. E., M. W. Evans, and B. L. Weber (1977), Ocean surface currents mapped by radar, *Science*, *198*, 138–144, doi:10.1126/science.198.4313.138.

Chen, C., R. Ji, L. Zheng, M. Zhu, and M. Rawson (1999), Influences of physical processes on the ecosystem in Jiaozhou Bay: A coupled physical and biological model experiment, *J. Geophys. Res.*, *104*(C12), 29,925–29,949, doi:10.1029/1999JC900203.

Csanady, G. T. (1976), Mean circulation in shallow seas, *J. Geophys. Res.*, *81*(30), 5389–5399, doi:10.1029/JC081i030p05389.

de Paolo, T., and E. Terrill (2007), Skill assessment of resolving ocean surface current structure using compact-antenna-style HF radar and the MUSIC direction-finding algorithm, *J. Atmos. Oceanic Technol.*, *24*, 1277–1300, doi:10.1175/JTECH2040.1.

Ding, W. A. (1992), Tides and tidal currents (in Chinese), in *Ecology and Living Resources of Jiaozhou Bay*, edited by R. Liu, pp. 39–72, Sci. Press, Beijing.

Ebuchi, N., Y. Fukamachi, K. I. Ohshima, K. Shirasawa, M. Ishikawa, T. Takatsuka, T. Daibo, and M. Wakatsuchi (2006), Observation of the Soya Warm Current using HF ocean radar, *J. Oceanogr.*, *62*, 47–61, doi:10.1007/s10872-006-0031-0.

Editorial Board of Annals of Bays in China (1993), *Annals of Bays in China, vol. 4, Southern Shandong Peninsular and Jiangsu Province* (in Chinese), pp. 157–258, China Ocean Press, Beijing.

Fang, G., Y. Wang, Z. Wei, B. H. Choi, X. Wang, and J. Wang (2004), Empirical cotidal charts of the Bohai, Yellow, and East China Seas from 10 years of TOPEX/Poseidon altimetry, *J. Geophys. Res.*, *109*, C11006, doi:10.1029/2004JC002484.

First Institute of Oceanography of SOA (1984), *Physical Environments of Jiaozhou Bay* (in Chinese), China Ocean Press, Beijing.

Jay, D. A., and J. D. Smith (1990), Residual circulation in shallow estuarines: 2. Weakly stratified and partially mixed, narrow estuaries, *J. Geophys. Res.*, *95*, 733–748, doi:10.1029/JC095iC01p00733.

Kaplan, D. M., J. Largier, and L. W. Botsford (2005), HF radar observations of surface circulation off Bodega Bay (northern California, USA), *J. Geophys. Res.*, *110*, C10020, doi:10.1029/2005JC002959.

Kohut, J., and S. Glenn (2003), Calibration of HF radar surface current measurement using measured antenna beam patterns, *J. Atmos. Oceanic Technol.*, *20*, 1303–1316, doi:10.1175/1520-0426(2003)020<1303:IHRSCM>2.0.CO;2.

Kudryavtsev, V., V. Shrira, V. Dulov, and V. Malinovsky (2008), On the vertical structure of wind-driven sea currents, *J. Phys. Oceanogr.*, *38*, 2121–2144, doi:10.1175/2008JPO3883.1.

Kundu, P. K. (1976), Ekman veering observed near the ocean bottom, *J. Phys. Oceanogr.*, *6*, 238–242, doi:10.1175/1520-0485(1976)006<0238:EVONTO>2.0.CO;2.

Large, W. G., and S. Pond (1981), Open ocean momentum flux measurements in moderate to strong winds, *J. Phys. Oceanogr.*, *11*, 324–336, doi:10.1175/1520-0485(1981)011<0324:OOMFMI>2.0.CO;2.

Lee, S.-H., and R. C. Beardsley (1999), Influence of stratification on residual tidal currents in the Yellow Sea, *J. Geophys. Res.*, *104*(C7), 15,679–15,701, doi:10.1029/1999JC900108.

Lentz, S. J. (2001), The influence of stratification on the wind-driven cross shelf circulation over the North Carolina Shelf, *J. Phys. Oceanogr.*, *31*(9), 2749–2760, doi:10.1175/1520-0485(2001)031<2749:TIOSOT>2.0.CO;2.

Lipa, B. J., and D. Barrick (1983), Least squares methods for the extraction of surface currents from CODAR crossed-loop data: Application at ARSLOE, *IEEE J. Oceanic Eng.*, *8*, 226–253, doi:10.1109/JOE.1983.1145578.

Liu, Z., H. Wei, G. Liu, and J. Zhang (2004), Simulation of water exchange in Jiaozhou Bay by average residence time approach, *Estuarine Coastal Shelf Sci.*, *61*, 25–35, doi:10.1016/j.ecss.2004.04.009.

Liu, Z., H. Wei, J. Bai, J. Zhang, D. Liu, and S. Liu (2007), Nutrients seasonal variation and budget in Jiaozhou Bay, China: A 3-dimensional physical–biological coupled model study, *Water Air Soil Pollut.*, *7*, 607–623, doi:10.1007/s11267-007-9128-8.

Lozovatsky, I., Z. Liu, H. Wei, and H. Fernando (2008a), Tides and mixing in the northwestern East China Sea part I: Rotating and reversing tidal flows, *Cont. Shelf Res.*, *28*, 318–337, doi:10.1016/j.csr.2007.08.006.

Lozovatsky, I., Z. Liu, H. Wei, and H. Fernando (2008b), Tides and mixing in the northwestern East China Sea part II: Near-bottom turbulence, *Cont. Shelf Res.*, *28*, 338–350, doi:10.1016/j.csr.2007.08.007.

Lü, X., and F. Qiao (2008), Distribution of sunken macroalgae against the background of tidal circulation in the coastal waters of Qingdao, China, in summer 2008, *Geophys. Res. Lett.*, *35*, L23614, doi:10.1029/2008GL036084.

Lü, X., F. Qiao, and C. Xia (2008), Numerical simulation of tides and three dimensional tidal currents in Jiaozhou Bay by a movable land-sea boundary model (in Chinese with English abstract), *Acta Oceanol. Sin.*, *30*, 21–29.

Lu, Y., F. Hua, Z. Wei, and B. Fan (2008), Preliminary analysis on residual current along the section across the Jiaozhou Bay mouth (in Chinese with English abstract), *Adv. Mar. Sci.*, *26*(3), 305–316.

Marine Environmental Monitoring Center (1992), A comprehensive environmental investigation and study on the Jiaozhou Bay and coastal area (in Chinese), *Mar. Sci. Bull.*, *11*(3), 1–76.

Paduan, J. D., and M. S. Cook (1997), Mapping surface currents in Monterey Bay with CODAR-type HF radar, *Oceanography*, *10*, 49–52.

Paduan, J. D., and H. C. Graber (1997), Introduction to high-frequency radar: Reality and myth, *Oceanography*, *10*, 36–39.

Paduan, J. D., and L. Rosenfeld (1996), Remotely sensed surface currents in Monterey Bay from shore-based HF radar (Coastal Ocean Dynamics Application Radar), *J. Geophys. Res.*, *101*, 20,669–20,686, doi:10.1029/96JC01663.

Paduan, J. D., D. E. Barrick, D. Fernandez, Z. Hallock, and C. Teague (2001), Improving the accuracy of coastal HF radar current mapping, *Hydrol. Int.*, *5*, 26–29.

Pan, Y., Y. Guo, and C. Zeng (1995), Annual primary production in the inlet of Jiaozhou Bay, China (in Chinese with English abstract), *Oceanol. Limnol. Sin.*, *26*(3), 309–316.

Pawlowicz, R., B. Beardsley, and S. Lentz (2002), Classical tidal harmonic analysis including error estimates in MATLAB using T-TIDE, *Comput. Geosci.*, *28*, 929–937, doi:10.1016/S0098-3004(02)00013-4.

Pu, S., J. Cheng, Y. Zhang, Q. Shi, J. Luo, and W. Fan (2004), Monsoon and annual variability of sea surface slope and their effects on alongshore current (in Chinese with English abstract), *Mar. Sci. Bull.*, *23*(2), 1–7.

Schmidt, R. O. (1986), Multiple emitter location and signal parameter estimation, *IEEE Trans. Antennas Propag.*, *34*(3), 276–280, doi:10.1109/TAP.1986.1143830.

Smith, S. (1988), Coefficients for sea surface wind stress, heat flux, and wind profiles as a function of wind speed and temperature, *J. Geophys. Res.*, *93*(C12), 15,467–15,472, doi:10.1029/JC093iC12p15467.

Son, Y., S. Lee, C. Kim, J. Lee, and G. Lee (2007), Surface current variability in the Keum River Estuary (South Korea) during summer 2002 as observed by high-frequency radar and coastal monitoring buoy, *Cont. Shelf Res.*, *27*, 43–63, doi:10.1016/j.csr.2006.08.008.

Stacey, M. T., M. L. Brennan, J. R. Burau, and S. G. Monismith (2010), The tidally averaged momentum valance in a partially and periodically stratified estuary, *J. Phys. Oceanogr.*, *40*, 2418–2434, doi:10.1175/2010JPO4389.1.

Sun, S., Y. Zhang, Y. Wu, G. Zhang, F. Zhang, and X. Pu (2005), Annual variation of primary productivity in Jiaozhou Bay (in Chinese), *Oceanol. Limnol. Sin.*, *36*(6), 481–486.

Visser, A. W., M. J. Bowman, and W. R. Crawford (1990), Dynamics of tidally forced basin-wide coastal eddies, in *Residual Currents and Long-Term Transport*, edited by R. T. Cheng, pp. 64–78, Springer, New York.

Wang, H., X. Fang, G. Kuang, D. Yang, and S. Chen (1980), The simulation of circulation and pollution diffusion in Jiaozhou Bay—I: Numerical study of tidal current (in Chinese), *J. Shandong Coll. Oceanol.*, *10*(1), 26–63.

Winant, C. D. (2008), Three-dimensional residual tidal circulation in an elongated, rotating basin, *J. Phys. Oceanogr.*, *38*, 1278–1295, doi:10.1175/2007JPO3819.1.

Xia, C., F. Qiao, Y. Yang, J. Ma, and Y. Yuan (2006), Three dimensional structure of the summertime circulation in the Yellow Sea from a wave-tide-circulation coupled model, *J. Geophys. Res.*, *111*, C11S03, doi:10.1029/2005JC003218.

Yan, J., H. Wang, and X. Bao (2001), The simulation of 3D tidal and residual current in Jiaozhou Bay (in Chinese), *Adv. Earth Sci.*, *16*(2), 172–177.

Yang, Y., and Y. Wu (1999), Temperature and salinity structures of Jiaozhou Bay waters during 1991–1995 (in Chinese with English abstract), *J. Oceanogr. Huanghai Bohai Seas*, *17*(3), 31–36.

Ye, A. L., and F. Q. Li (1991), *Physical Oceanography* (in Chinese), Ocean Univ. of Qingdao Press, Qingdao, China.

Yoshikawa, Y., T. Matsuno, K. Marubayashi, and K. Fukudome (2007), A surface velocity spiral observed with ADCP and HF radar in the Tsushima Strait, *J. Geophys. Res.*, *112*, C06022, doi:10.1029/2006JC003625.

Zhang, J., and Z. Sheng (1997), A study of changes in nutrient structure of Jiaozhou Bay (in Chinese with English abstract), *Oceanol. Limnol. Sin.*, *28*(5), 529–535.

Zhao, B. R. (1982), A study about influence of local wind on coastal current over Yellow Sea and East China Sea (in Chinese), *Oceanol. Limnol. Sin.*, *13*(6), 479–488.

J. Chen and X. Chen (corresponding author), College of Physical and Environmental Oceanography, Ocean University of China, Qingdao 266100, China. (xchen@ouc.edu.cn)

M. Guo and W. Hu, North China Sea Marine Forecasting Center, State Oceanic Administration, Qingdao 266033, China.

J. Zhao, Division of Meteorology and Physical Oceanography, Rosenstiel School of Marine and Atmospheric Science, University of Miami, Miami, FL 33149, USA.